International Journal of Nanomedicine

Dovepress

open access to scientific and medical research

Open Access Full Text Article

ORIGINAL RESEARCH

Microwave-assisted synthesis of SnO_2 nanorods for oxygen gas sensing at room temperature

This article was published in the following Dove Press journal:
International Journal of Nanomedicine
8 October 2013
Number of times this article has been viewed

Ameer Azam[1]
Sami S Habib[1]
Numan A Salah[1]
Faheem Ahmed[2]

[1]Centre of Nanotechnology, King Abdulaziz University, Jeddah, Saudi Arabia; [2]School of Nano and Advanced Materials Engineering, Changwon National University, Changwon, South Korea

Abstract: High-quality single-crystalline SnO_2 nanorods were synthesized using a microwave-assisted solution method. The nanorods were characterized using X-ray diffraction (XRD), field-emission scanning electron microscopy (FE-SEM), transmission electron microscopy (TEM), ultraviolet-visible and Raman spectroscopy, Brunauer–Emmett–Teller (BET), and electrical resistance measurements. The XRD pattern indicated the formation of single-phase SnO_2 nanorods with rutile structure. FE-SEM and TEM images revealed tetragonal nanorods of about 450–500 nm in length and 60–80 nm in diameter. The nanorods showed a higher BET surface area of 288 m^2/g, much higher than that of previously reported work. The Raman scattering spectra indicated a typical rutile phase of the SnO_2. The absorption spectrum showed an absorption peak centered at 340 nm, and the band-gap value was found to be 3.64 eV. The gas-sensing properties of the SnO_2 nanorods for oxygen gas with different concentrations were measured at room temperature. It was found that the value of resistance increased with the increase in oxygen gas concentration in the test chamber. The SnO_2 nanorods exhibited high sensitivity and rapid response-recovery characteristics to oxygen gas, and could detect oxygen concentration as low as 1, 3, 5, and 10 ppm.

Keywords: SnO_2, nanorods, microwave, gas sensor

Introduction

During the past decade, metal oxide semiconductor material-based gas sensors have attracted extensive attention.[1] Among them, as an *n*-type wide band-gap semiconductor, SnO_2 is regarded as one of the promising materials for gas sensing because of its excellent characteristics, such as low cost, high sensitivity, rapid response, and fast recovery.[2,3] In addition, it has potential applications in detecting polluted or toxic gases and other species,[4–6] as well as successful use in optoelectronic devices.[7–13] Oxygen gas monitoring is an important issue in various fields, such as the environment, transportation, medicine, and agriculture.[14,15] Metal oxide semiconductor gas sensors offer an inexpensive and simple method for monitoring gases, due to low cost, small size, and real-time detection.[16–18] Oxygen gas sensors have been widely used in industrial heating furnaces, to monitor such environments as underground mines and oil fields, and to prevent gas poisoning. However, most sensors made from semiconducting oxide materials have a high operating temperature, which is becoming an obstacle to their application in different areas. Additionally, 1-D nanostructures, including nanorods, nanowires, nanotubes, and nanobelts, are excellent candidates for chemical sensing purposes,[19–22] because of their ultrahigh surface-to-volume ratio, high sensitivity, and short response time to chemical surroundings. Due to high surface-to-volume ratios of

Correspondence: Ameer Azam
Centre of Nanotechnology,
King Abdulaziz University,
PO Box 80200, Jeddah 21589,
Saudi Arabia
Tel +966 53 118 5621
Fax +966 2 695 1566
Email azam222@rediffmail.com

these 1-D nanostructures, their first major application was in chemical/gas sensors, as was demonstrated with SnO_2-coated carbon nanotubes,[23] functionalized silicon nanowires,[24] and SnO_2 nanowires/nanowhiskers.[25,26] It has been reported that a gas sensor is a chemical sensor that converts chemical information, which is determined by different concentrations of gaseous chemical species, into an electrical signal.[27] Thus, a chemical gas sensor gives an electrical signal that can be related to the chemical environment if it is exposed to gas in some way. The sensor response in most cases is defined as difference or ratio between the steady-state sensor response when exposed to the sample gas and the sensor response when exposed to a reference atmosphere (not sample gas). The concentration-versus-response relationship for most gas sensors approximately exhibits either saturated linear behavior (ie, linear for low concentrations and saturated for higher concentrations) or logarithmic behavior. However, most of the drawbacks of commonly used gas-sensing technologies come from their lack of stability. There are other demands to be met while producing gas sensors, such as short response time, good reversibility, low cost, small size, and low power consumption. In general, oxygen-related gas-sensing mechanisms involve chemisorptions of oxygen on the oxide surface followed by charge transfer during the reaction between chemisorbed oxygen-reducing and target-gas molecules. To reveal the mechanism of gas sensors, many models, such as the point-contact model,[28] face-contact model,[29] and surface-depletion model,[2,3,30] have been established. These models emphasize the importance of charge transfer in the sensing mechanism. They can illustrate this adsorption process qualitatively, but it is difficult to predict sensing results of gas sensors.

Much effort has been focused on the fabrication of nanostructured SnO_2 by employing various techniques, such as the molten-salt method, hydrothermal method, laser-ablation deposition, and direct oxidation growth.[31–41] However, it still remains a great challenge to find reliable techniques with low cost for the fabrication of low-dimensional SnO_2 nanostructures. In comparison to other approaches, the solution method has its own advantages, such as low temperature, high production yield, and high quality. Nowadays, a new method – microwave-assisted synthesis – is being used for the synthesis of nanomaterials. Due to this method's unique features, such as short reaction time, enhanced reaction selectivity, energy saving, and high reaction rate,[42,43] its use has been rapidly increasing.[43–47] Microwave heating not only reduces the chemical reaction times by several orders of magnitude but also suppresses side reactions, and thus improves the yield and reproducibility of a specific synthesis protocol. All these features represent important parameters that have to be considered during the development of "greener" synthesis methodologies, and therefore it can be expected that the microwave technique will also play a fundamental role in a future environmentally friendlier "synthetic nanotechnology."

In this paper, we report the low-concentration detection of oxygen gas at room temperature using SnO_2 nanorods prepared by the microwave-assisted solution method. Synthesized SnO_2 nanorods showed excellent gas sensitivity, and the reported technique is fast and cost-effective, which is important for large-scale applications in gas sensors and can be applicable at the industrial level.

Materials and methods

All of the reagents involved in the experiments were of analytical grade and utilized as received without further purification. The synthesis was carried out in a domestic microwave oven. In a typical synthesis, an equal (0.05 M) molar ratio of $SnCl_2$:$2H_2O$ (99.99%, Sigma-Aldrich, St Louis, MO, USA) and NaOH (99.99%, Sigma-Aldrich) was dissolved in 50 mL deionized water in a round-bottom flask, and the solution was put into a microwave oven and treated at a power of 300 W for 20 minutes. After microwave processing, the solution was cooled down to room temperature. The resulting precipitate was separated by centrifugation, then washed with deionized water and absolute ethanol several times, and finally dried in an oven at 80°C for 24 hours. Prior to the characterization, the samples were annealed at different temperatures (400°C and 600°C) for 2 hours.

X-ray diffraction (XRD) measurements were carried out using an X-ray diffractometer with Cu Kα radiation (λ =1.5406 Å) operated at a voltage of 40 kV and current of 30 mA. The morphologies were investigated on a field-emission scanning electron microscope (FE-SEM). The elemental composition of the SnO_2 was determined by energy-dispersive X-ray spectroscopy (EDX) attached to the FE-SEM. Transmission electron microscopy (TEM) images, selected-area electron diffraction (SAED) patterns, and high-resolution TEM (HR-TEM) images were obtained by FE-TEM operated at 200 kV. For the TEM observation, the samples were collected on a carbon holey grid. The room-temperature optical absorption spectrum was recorded in the range of 200–800 nm using an ultraviolet-visible (UV-vis) spectrophotometer. In order to get the phonon vibrational study of the SnO_2 nanorods, a micro-Raman spectrometer was used with a 532 nm solid-state primary laser as an

excitation source in the backscattering configuration at room temperature. The Brunauer–Emmett–Teller (BET) specific surface-area measurements were carried out by nitrogen adsorption using an Autosorb®-1 (Quantachrome Instruments, Boynton Beach, FL, USA).

Gas-sensing properties of the SnO_2 nanorods were examined for the O_2 gas at room temperature. For gas-sensing measurements, the sensor was put in a test chamber. High-purity O_2 gas was passed through the test chamber at different flow rates controlled by a mass flow controller. The sample resistance of the SnO_2 nanorods sensor was measured using an HP (Palo Alto, CA, USA) 34401 multimeter as a function of time, which was interfaced with a personal computer through a general-purpose interface bus card. From these measurements, gas-sensor parameters, including sensitivity, response and recovery times, were determined.

Results and discussion

Figure 1 shows the XRD patterns of the as-prepared and annealed samples of SnO_2 at different temperatures. In this experiment, $SnCl_2$ was used as the precursor, which eventually underwent oxidation to form SnO_2 under the microwave condition. Before oxidation, Sn was found to be in the form of hydroxide intermediate $Sn_6O_4(OH)_4$, which was explicitly revealed by XRD (see Figure 1). XRD patterns indicated that for the as-prepared sample, the precursor $SnCl_2$ mainly transformed into poorly crystallized $Sn_6O_4(OH)_4$ (International Centre for Diffraction Data [ICDD] 46-1486). It can be seen that as the annealing temperature increases to 400°C, the diffraction peaks of $Sn_6O_4(OH)_4$ gradually vanish, and at 600°C, rutile SnO_2 was formed. All the diffraction peaks of the sample annealed at 600°C are indexed to tetragonal SnO_2 with a rutile structure with lattice parameters of a =4.7390 Å and c =3.1861 Å. These results are very well matched with the ICDD card 41-1445. The sharpness of the peaks shows the high crystallinity of the prepared samples.

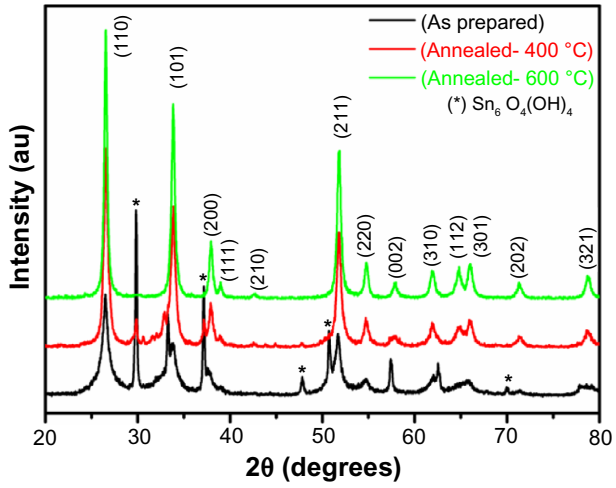

Figure 1 X-ray diffraction patterns of as-prepared and annealed SnO_2 samples.

Figure 2A shows the FE-SEM image of the SnO_2 nanorods annealed at 600°C for 2 hours. The nanorods have a uniform length of about 450–500 nm and a diameter of about 60–80 nm. TEM and HR-TEM investigations give further insight into the morphologies and the structural features of SnO_2 nanorods. The TEM image in Figure 2B shows that the nanorods are needle-like, with a diameter of 50 nm at the tip and 75 nm in the middle, and a length of about 500 nm. The clear lattice fringes in the HR-TEM images (Figure 2C) show the single crystal nature of the SnO_2 nanorods. The spacing between two adjacent lattice planes is 0.33 nm, corresponding to the (110) planes of SnO_2, which indicates that the nanorods are bound by (110) facets. Therefore, the [001] direction is the favored growth direction for the nanorods, which is further confirmed by the SAED pattern taken from individual nanorods (inset of Figure 2C).

The elemental composition of the SnO_2 nanorods was determined by EDX. Figure 2D shows the corresponding EDX spectrum of the annealed SnO_2 nanorods. The EDX analysis of these nanorods demonstrates that the nanorods are only composed of elemental Sn and O.

The formation of a tetragonal rutile structure of SnO_2 nanorods was further supported by Raman spectra employed at room temperature. The rutile structure SnO_2 belongs to the space group $P4_2/mnm$,[48–50] with Sn and O atoms in 2*a* and 4*f* positions, respectively. Figure 3 shows the Raman spectrum of the SnO_2 nanorods in the wave-number range 300–850 cm^{-1}. The Raman spectrum of the SnO_2 nanorods shows conventional vibration modes[49–52] of E_g, $(A_{2u})V_{(TO)}$, A_{1g}, $(A_{2u})V_{(LO)}$, and B_{2g} centered at 473 cm^{-1}, 498 cm^{-1}, 629 cm^{-1}, 689 cm^{-1}, and 770 cm^{-1}, respectively. This is in agreement with the results of group-theory analysis.[53,48]

In order to study the optical properties of SnO_2 nanorods, UV-vis spectroscopy was used. The UV-vis absorption spectrum of SnO_2 nanorods annealed at 600 for 2 hours is presented in Figure 4. It is clear from the absorption spectrum that there is a strong absorption peak positioned at 340 nm. It is well known that the theory of optical absorption gives the relationship between the absorption coefficients α and the photon energy $h\nu$ for direct allowed transition as[54]:

$$(\alpha h\nu)^2 = \mathrm{A}\,(h\nu - E_g) \quad (1)$$

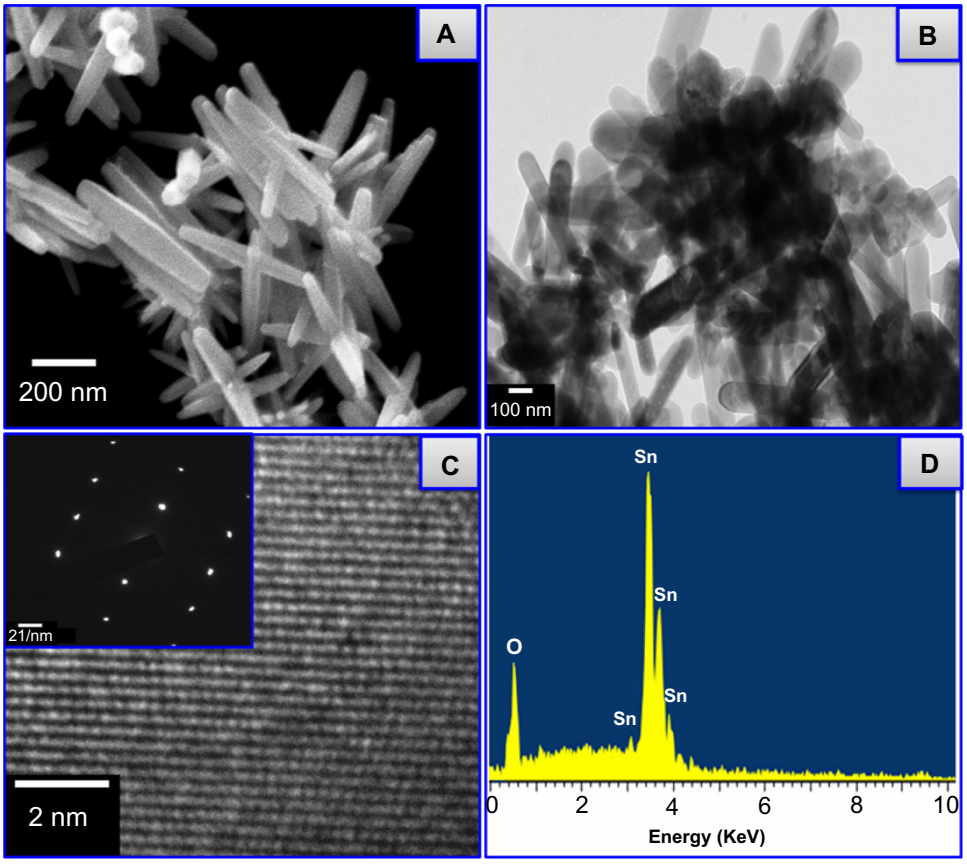

Figure 2 (**A**) Field emission scanning electron microscopy image, (**B**) transmission electron microscopy (TEM) image, (**C**) high-resolution TEM (HRTEM) image, and (**D**) energy-dispersive X-ray spectroscopy spectrum of SnO_2 nanorods annealed at 600°C for 2 hours. Inset of (**C**) shows corresponding selected-area electron diffraction pattern.

where A is a constant characteristic of the semiconductor, $h\nu$ is the photon energy, E_g is the apparent optical band gap, and α is the absorption coefficient. The direct band gap is determined using this equation when the straight portion of the $(\alpha h\nu)^2$ against the $h\nu$ plot is extrapolated to intersect the energy axis at $\alpha = 0$. The inset of Figure 4 shows the plot of $(\alpha h\nu)^2$ versus $h\nu$ for SnO_2 nanorods. The E_g value of the SnO_2 nanorods was determined from the intercept of $(\alpha h\nu)^2$ versus $(h\nu)$ curves and found to be 3.64 eV. It is clear that the optical band gap is larger than the value of 3.62 eV for bulk SnO_2.

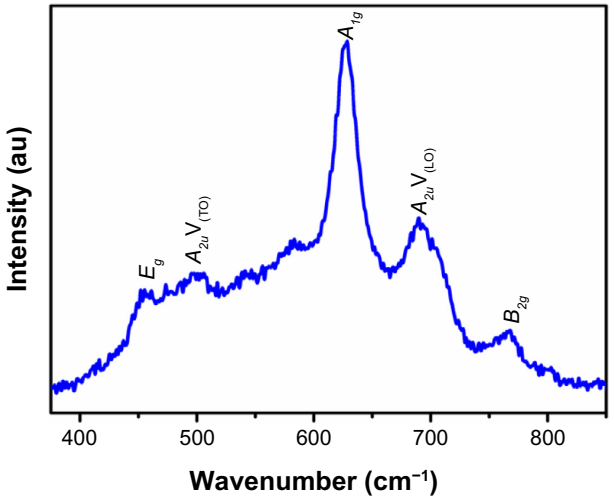

Figure 3 Room-temperature Raman spectrum of SnO_2 nanorods annealed at 600°C for 2 hours.

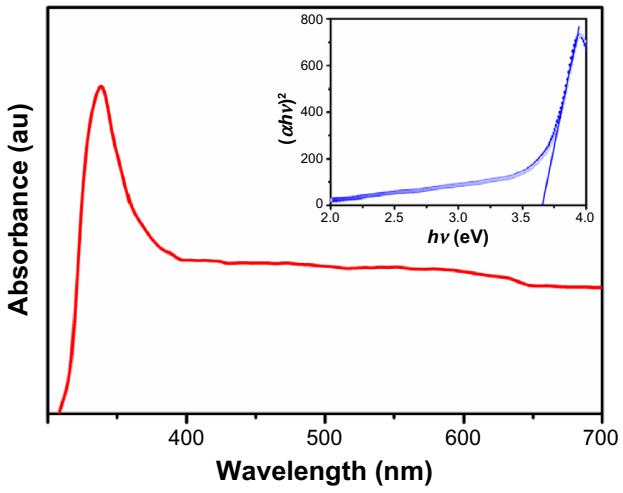

Figure 4 Room-temperature absorption spectrum of SnO_2 nanorods annealed at 600°C for 2 hours. Inset shows corresponding optical band-gap plot.

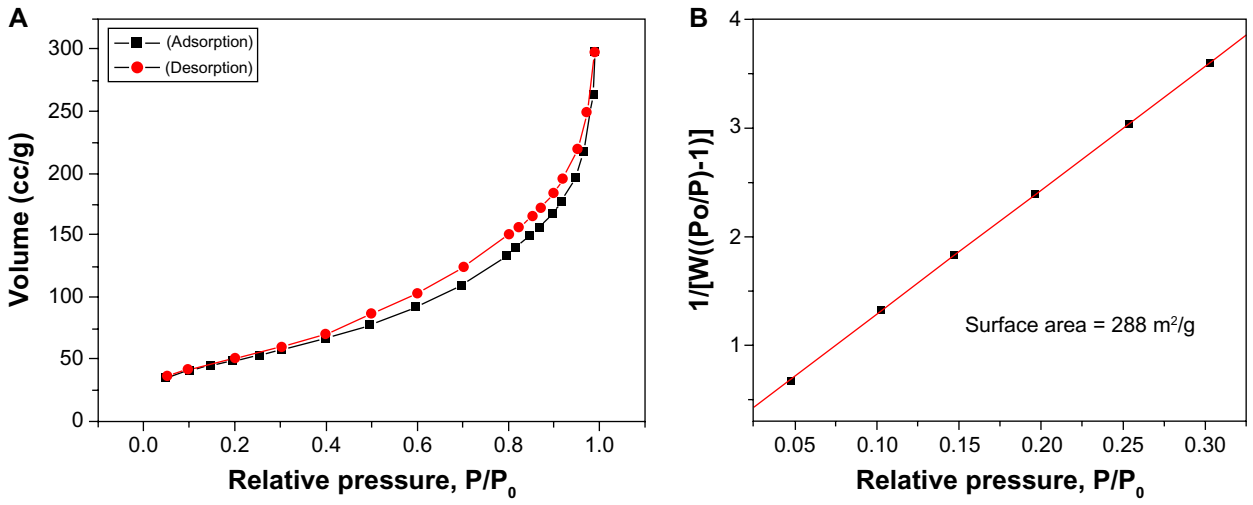

Figure 5 (**A**) Nitrogen adsorption–desorption isotherm of SnO_2 nanorods annealed at 600°C for 2 hours; (**B**) corresponding Brunauer–Emmett–Teller surface-area plot.

Figure 5 gives the nitrogen adsorption–desorption isotherm and the surface-area plot of the annealed SnO_2 nanorods. The isotherm shows that nitrogen-adsorption volume gradually increased as relative pressure increased and then decreased as relative pressure decreased (Figure 5A). The BET surface area of the annealed SnO_2 nanorods was found to be 288 m^2/g. The SnO_2 nanorods (prepared by this method) showed higher surface area than other reported SnO_2 nanostructures (mesoporous, nanotubes, nanosheet, nanowires).[55,56] It was also much higher than commercially produced SnO_2 nanoparticles, such as SnO_2 (BET 47.2 m^2/g, 18.3 nm in diameter, 549657-25 G; Sigma-Aldrich), SnO_2 (BET 25.9 m^2/g, 34 nm in diameter; Yamanaka, Osaka, Japan), SnO_2 (BET 23 m^2/g, 26 nm in diameter, 37314-13, NanoTek®; CI Kasei, Tokyo, Japan) or In_2O_3–SnO_2 (BET 3–6 m^2/g, 100–300 nm in diameter; Sumitomo Chemical, Tokyo, Japan).

Figure 6 shows the response-recovery characteristics for the SnO_2 nanorod sensors operated at room temperature under different oxygen gas concentrations. Figure 6 depicts the change in resistance as a function of time with different oxygen concentrations ranging from 1 to 10 ppm. The sensor clearly shares a common feature at all concentrations, wherein resistance increases sharply when the oxygen gas is on, yet returns to its original state when the oxygen gas is off. SnO_2 is known to be of an *n*-type semiconducting nature, and its sensing properties are controlled exclusively by a change in surface resistance. Therefore, the species and amount of the chemisorbed oxygen species on the oxide surface play an important role in influencing the functionality.[57–59] In general, sensing materials with low-dimensional structures should have a large surface area, which could not only provide more adsorption sites for the oxygen species and the tested gases but also facilitate the interaction between the oxide surfaces and gas molecules.[60] This induces a more significant degree of electron transfer, and hence more pronounced output of electric signal, which is detected by the electric circuit.

The mechanism of sensing of SnO_2 nanorod sensors can be explained by the modulation model of the depletion layer.[61] The electrical conductance of nanorods is determined by the amount of electrons in a conduction band of nanorods. The more electrons are present inside the rod, the higher the conductivity the nanorods possess. If the surrounding analyte gas molecules are not absorbed at all by the nanorods, there is no electron exchange between the nanorods and the gas molecules. Hence, the conductivity of the nanorods remains at the same level as without the gas surroundings. On the other hand, when an SnO_2 nanorod sensor is exposed to

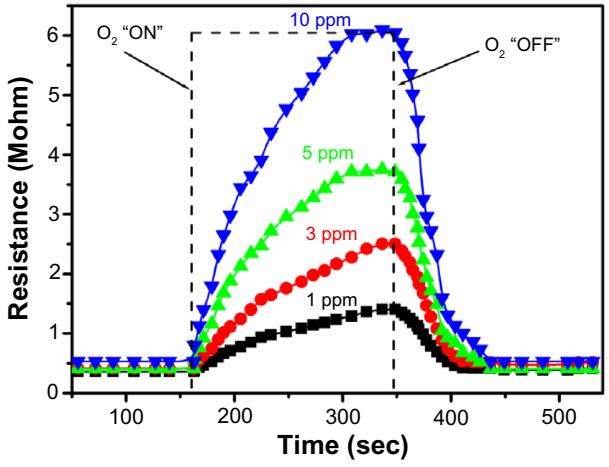

Figure 6 Plot of change in resistance of SnO_2 nanorod gas sensors for different oxygen concentrations.

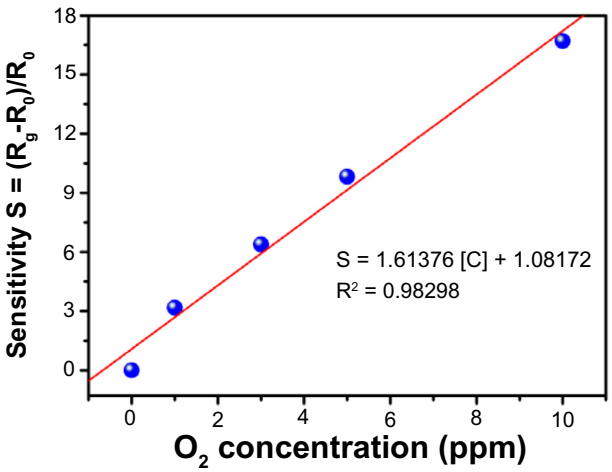

Figure 7 Plot of sensitivity as a function of oxygen concentration.

oxygen gas, oxygen molecules are captured by the surface electrons and become adsorbed oxygen. The adsorbed oxygen creates a depletion layer on the surface of the nanorods and increases the energy barrier, thereby increasing the electrical resistance of the nanorods. For gas-sensor applications, the larger the variation in the resistance, the higher the sensitivity that can be achieved. The gas sensitivity (S) was estimated using the relationship $S = (R_g - R_0)/R_0$, where R_0 is the initial resistance in the absence of oxygen gas, and R_g is the resistance measured in the presence of oxygen gas. Figure 7 shows the sensitivities calculated from Figure 6 for different oxygen concentrations. It is clear from Figure 7 that the sensitivity increases with increasing oxygen gas concentration, hence a linear relationship is obtained between sensitivity and oxygen gas concentration. The enhanced sensitivity at room temperature as operating temperature is attributed to the higher surface-to-volume ratio of the nanorods. Larger surface-to-volume ratio of nanorods creates more oxygen adsorption and increases the resistance of the material, as shown in Figure 7. Hence, the increase in resistance generates a corresponding increase in the sensor's sensitivity.

Conclusion

In summary, we have successfully fabricated a sensor made of SnO_2 nanorods by a rapid and cost-effective microwave-assisted solution method and investigated its gas-sensing properties. XRD, SAED, HR-TEM, and Raman analyses revealed that the SnO_2 nanorods annealed at 600°C for 2 hours have a single-crystalline nature with rutile structure. FE-SEM and TEM images show that the SnO_2 nanorods have length ~500 nm and diameter of ~80 nm, respectively. BET analysis showed that SnO_2 nanorods had surface area of 288 m^2/g, which was much higher than that of the SnO_2 reported earlier or commercially produced nanoparticles. The UV-vis spectrum showed the maximum absorption band at 340 nm and optical band gap of 3.64 eV. The SnO_2 nanorod-based oxygen gas sensor operated at room temperature showed good sensitivity for various concentrations of oxygen gas. The sensitivity of the gas sensor is linearly proportional to oxygen concentrations ranging from 1 to 10 ppm. The present SnO_2 nanorod gas sensor represents an important step forward in exploring gas sensors that can be operated at room temperature for future practical applications.

Acknowledgment

This project was funded by the Deanship of Scientific Research (DSR), King Abdulaziz University, Jeddah, under grant 224/903/1433. The authors therefore acknowledge with thanks DSR technical and financial support.

Disclosure

The authors report no conflicts of interest in this work.

References

1. Azad AM, Akbar SA, Mhaisalkar SG, Birkefeld LD, Goto KS. Solid-State Gas Sensors [review]. *J Electrochem Soc*. 1992;139:3690–3704.
2. Chen YJ, Xue XY, Wang YG, Wang TH. Synthesis and ethanol sensing characteristics of single crystalline SnO_2 nanorods. *Appl Phys Lett*. 2005;87:233503.
3. Li CC, Du ZF, Li LM, Yu HC, Wan Q, Wang TH. Surface-depletion controlled gas sensing of ZnO nanorods grown at room temperature. *Appl Phys Lett*. 2007;91:032101.
4. Chen YJ, Nie L, Xue XY, Wang YG, Wang TH. Linear ethanol sensing of SnO_2 nanorods with extremely high sensitivity. *Appl Phys Lett*. 2006;88:083105.
5. Devi GS, Subrahmanyam V , Gadkari SC, Gupta SK. NH_3 gas sensing properties of nanocrystalline ZnO based thick films. *Anal Chim Acta*. 2006;568:41–46.
6. Moon WJ, Yu JH, Choi GM. The CO and H_2 gas selectivity of CuO-doped SnO_2–ZnO composite gas sensor. *Sens Actuators B*. 2002;87:464–470.
7. Veglieri GS. Classical and novel techniques for the preparation of SnO_2 thin-film gas sensors. *Sens Actuators B*. 1992;6:239.
8. Dieguez A, Rodriguez AR, Morante JR. Morphological analysis of nanocrystalline SnO_2 for gas sensor applications. *Sens Actuators B*. 1996;31:1.
9. Ferrere S, Zaban A, Gregg BA. Dye Sensitization of Nanocrystalline Tin Oxide by Perylene Derivatives. *J Phys Chem B*. 1997;101:4490.
10. He YS, Campbell JC, Murphy RC. Electrical and optical characterization of Sb: SnO_2. *J Mater Res*. 1993;8:3131.
11. Jarzebski ZM, Maraton JP. Physical Properties of SnO_2 Materials. *J Electrochem Soc*. 1976;123:199.
12. Vasu V, Subrahmanyam A. Electrical and optical properties of sprayed SnO_2 films: Dependence on the oxiding agent in the starting material. *Thin Solid Films*. 1990;193:973.
13. Tsunashima A. Preparation and properties of antimony-doped SnO_2 films by thermal decomposition of tin 2-ethylhexanoate. *J Mater Sci*. 1986;21:2731.
14. Yamazoe N, Miura N. Development of gas sensors for environmental protection. *IEEE Tran Compou Packag Manuf Technol Part A*. 1995;18:252–256.

15. Weppner W. Advanced principles of sensors based on solid state ionics. *Mater Sci Eng B*. 1992;15:48.
16. Korotcenkov G. Gas response control through structural and chemical modification of metal oxide films: state of the art and approaches. *Sens Actuators B*. 2005;107:209.
17. Barsan N, Koziej D, Weimar U. Metal oxide-based gas sensor research: How to? *Sens Actuators B*. 2007;121:18.
18. Dirksen JA, Duval K, Ring TA. NiO thin-film formaldehyde gas sensor. *Sens Actuators B*. 2001;80:106.
19. Huang XJ, Choi YK. Chemical sensors based on nanostructured materials. *Sens Actuators B*. 2007;122:659.
20. Kolmakov A, Chen X, Moscovits M. Functionalizing Nanowires with Catalytic Nanoparticles for Gas Sensing Application. *J Nanosci Nanotechnol*. 2008;8:111.
21. Huang XJ, Choi YK. Chemical sensors based on nanostructured materials. *Sens Actuators B*. 2007;122:659.
22. Strelcov E, Lilach Y, Kolmakov A. Gas Sensor Based on Metal-Insulator Transition in VO_2 Nanowire Thermistor. *Nano Lett*. 2009;9:2322.
23. Liang YX, Chen YJ, Wang TH. Low-resistance gas sensors fabricated from multiwalled carbon nanotubes coated with a thin tin oxide layer. *Appl Phys Lett*. 2004;85:666.
24. Cui Y, Wei Q, Park H, Lieber CM. Nanowire Nanosensors for Highly Sensitive and Selective Detection of Biological and Chemical Species. *Science*. 2001;293:1289.
25. Comini E, Faglia G, Sberveglieri G, Pan Z, Wang ZL. Stable and highly sensitive gas sensors based on semiconducting oxide nanobelts. *Appl Phys Lett*. 2002;81:1869.
26. Ying Z, Wan Q, Song ZT, Feng SL. SnO2 nanowhiskers and their ethanol sensing characteristics. *Nanotechnology*. 2004;15:1682.
27. Göpel W, Jones TA, Kleitz M, Lundström I, Seiyama T, editors. *Chemical and Biochemical Sensors*, Part I. Germany: VCH, Weinheim; 1991.
28. Feng P, Wan Q, Wang TH. Contact-controlled sensing properties of flowerlike ZnO nanostructures. *Appl Phys Lett*. 2005;87:213111.
29. Feng P, Xue XY, Liu YG, Wang TH. Highly sensitive ethanol sensors based on {100}-bounded In_2O_3 nanocrystals due to face contact. *Appl Phys Lett*. 2006;89:243514.
30. Dayan NJ, Sainkar SR, Karekar RN, Aiyer RC. Formulation and characterization of ZnO:Sb thick-film gas sensors. *Thin Solid Films*. 1998;325:254–258.
31. Wang WZ, Xu CK, Wang GH, Liu YK, Zheng CL. Synthesis and Raman scattering study of rutile SnO_2 nanowires. *J Appl Phys*. 2002;92:2740.
32. Xu CK, Zhao XL, Liu S, Wang GH. Large-scale synthesis of rutile SnO_2 nanorods. *Solid State Commun*. 2003;125:301.
33. Liu ZQ, Zhang DH, Han S, et al. Laser Ablation Synthesis and Electron Transport Studies of Tin Oxide Nanowires. *Adv Mater*. 2003;15:1754.
34. Hu JQ, Yoshio B, Liu QL, Golberg D. Laser-Ablation Growth and Optical Properties of Wide and Long Single-Crystal SnO_2 Ribbons. *Adv Funct Mater*. 2003;13:493.
35. Cheng B, Russel JM, Shi WS, Zhang L, Samulski ET. Large-Scale, Solution-Phase Growth of Single-Crystalline SnO_2 Nanorods. *J Am Chem Soc*. 2004;126:5972.
36. Pan ZW, Dai ZR, Wang ZL. Nanobelts of Semiconducting Oxides. *Science*. 2001;291:1947.
37. Kong XH, Sun XM, Li YD. Synthesis of ZnO nanobelts by carbothermal reduction and their Photoluminescence properties. *Chem Lett*. 2003;32:546.
38. Dai ZR, Gole JL, Stout JD. Tin Oxide Nanowires, Nanoribbons, and Nanotubes. *J Phys Chem B*. 2002;106:1274.
39. Wang YL, Jiang XC, Xia YN. A Solution-Phase, Precursor Route to Polycrystalline SnO_2 Nanowires That Can Be Used for Gas Sensing under Ambient Conditions. *J Am Chem Soc*. 2003;125:16176.
40. Sun SH, Meng GW, Zhang MG, An XH, Wu GS, Zhang LD. Synthesis of SnO_2 nanostructures by carbothermal reduction of SnO_2 powder. *J Phys D Appl Phys*. 2004;37:409.
41. Hu JQ, Yoshio B, Golberg D. Self-catalyst growth and optical properties of novel SnO_2 fishbone-like nanoribbons. *Chem Phys Lett*. 2003;372:758.
42. Ela SE, Cogal S, Icli S. Conventional and microwave-assisted synthesis of ZnO nanorods and effects of PEG400 as a surfactant on the morphology. *Inorg Chim Acta*. 2009;362:1855
43. Krishnakumar T, Jayaprakash R, Pinna N, Singh VN, Mehta BR, Phani AR. Microwave-assisted synthesis and characterization of flower shaped zinc oxide nanostructures. *Mater Lett*. 2009;63:242.
44. Liu JS, Cao JM, Li ZQ, Ji GB, Zheng MB. A simple microwave-assisted decomposing route for synthesis of ZnO nanorods in the presence of PEG400. *Mater Lett*. 2007;61:4409.
45. Wang X, Jia J, Zhao L, Sun T. Chemisorption of hydrogen sulphide on zinc oxide modified aluminum-substituted SBA-15. *Appl Surf Sci*. 2008;254:5445.
46. Ma MG, Zhu YJ, Cheng GF, Huang YH. Microwave synthesis and characterization of ZnO with various morphologies. *Mater Lett*. 2008;62:507.
47. Hammarberg E, Schwab AP, Feldmann CJ. Microwave-assisted polyol synthesis of aluminium- and indium-doped ZnO nanocrystals. *Colloid Interface Sci*. 2009;29:334.
48. Kravets VG. Photoluminescence and Raman spectra of SnO_x nanostructures doped with Sm ions. *Opt Spectrosc*. 2007;103:766.
49. Peercy PS, Morosin B. Pressure and Temperature Dependences of the Raman-Active Phonons in SnO_2. *Phys Rev B*. 1973;7:2779.
50. Traylor JG, Smith HG, Nicklow RM, Wilkinson MK. Lattice Dynamics of Rutile. *Phys Rev B*. 1971;3:3457.
51. Chen ZW, Lai JKL, Shek CH. Insights into microstructural evolution from nanocrystalline SnO_2 thin films prepared by pulsed laser deposition. *Phys Rev B*. 2004;70:165314.
52. Katiyars RS, Dawsons P, Hargreaves MM, Wilkinson GR. Dynamics of the rutile structure. III. Lattice dynamics, infrared and Raman spectra of SnO_2. *J Phys C: Solid State Phys*. 1971;4:2421.
53. Kohno H, Iwasaki T, Mita Y, Takeda S. One-phonon Raman scattering studies of chains of crystalline-Si nanospheres. *J Appl Phys*. 2002;91:3232.
54. Mills G, Li ZG, Meisel D. Photochemistry and spectroscopy of colloidal arsenic sesquisulfide. *J Phys Chem*. 1988;92:822.
55. Masuda Y, Kato K. Aqueous synthesis of nanosheet assembled tin oxide particles and their N_2 adsorption characteristics. *J Cryst Growth*. 2009;311:593.
56. Masuda Y, Ohji T, Kato K. Highly Enhanced Surface Area of Tin Oxide Nanocrystals. *J Am Ceram Soc*. 2010;93(8):2140.
57. Sahm T, Gurlo A, Barsan N, Weimar U. Basics of oxygen and SnO_2 interaction; work function change and conductivity measurements. *Sens Actuators B*. 2006;118:78–83.
58. Barsan N, Koziej D, Weimar U. Metal oxide-based gas sensor research: How to? *Sens Actuators B*. 2007;121:18–35.
59. Barsan N, Weimar U. Conduction Model of Metal Oxide Gas Sensors. *J Electroceram*. 2001;7:143–167.
60. Mu Q, Li Y, Zhang Q, Wang H. Template-free formation of vertically oriented TiO_2 nanorods with uniform distribution for organics-sensing application. *J Hazard Mater*. 2011;188:363–368.
61. Gergintschew Z, Forster H, Kositza J, Schipanski D. Two-dimensional numerical simulation of semiconductor gas sensors. *Sens Actuators B*. 1995;170:26–27.